Review Article

State-of-the-art and challenges of non-destructive techniques for in-situ radiological characterization of nuclear facilities to be dismantled

Khalil Amgarou [a, *], Margarita Herranz [b]

[a] Commissariat à l'énergie atomique et aux énergies alternatives (CEA), DES/DDSD/DTPI/STRD/GRDT, Marcoule, BP 17171, 30207, Bagnols sur Cèze, Cedex, France
[b] Nuclear Engineering and Fluid Mechanics Department. University of the Basque Country (UPV/EHU), Pza Ingeniero Torres Quevedo,1, 48013, Bilbao, Spain

ARTICLE INFO

ABSTRACT

This paper reports on the state-of-the-art of the main non-destructive assay (NDA) techniques usually used for in-situ radiological characterization of nuclear facilities subject to a decommissioning programme. For the sake of clarity and coherence, they have been classified as environmental radiation monitoring, surface contamination measurements, gamma spectrometry, passive neutron counting and radiation cameras. Particular mention is also made here to the various challenges that each of these techniques must currently overcome, together with the formulation of some proposals for a potential evolution in the future.

1. Introduction

Decommissioning of nuclear facilities (power reactors, open or closed fuel cycle plants, research or medical accelerators, etc.) refers to the final step, after shutdown, in their life cycle and covers the whole process whereby the considered site is properly removed and its near environment restored to a predetermined endpoint, namely an unrestricted and unconditional release or future reuse [1,2]. It is hence essential to act on the upstream stage of every decommissioning programme for the optimum definition of viable and cost-effective dismantling scenarios, as well as for the safe classification and segregation of all radioactive wastes. This undoubtedly constitutes a complex issue, considering the wide variety of involved structures and equipment. For that reason, their proper in-situ radiological characterisation by means of non-destructive assay (NDA) techniques, in combination with any historical information and laboratory analysis of representative samples taken from specific locations, becomes a necessary prerequisite for a successful quantification of the different contaminated materials before starting the dismantling activities [3]. The main NDA instruments used in this domain are based on the detection of the different types of ionizing radiation, such as alpha (α), beta (β),

energetic photons (X- or γ-rays) and neutrons, emitted by the sought radionuclides in the item of interest, without affecting the physical or chemical form of this latter.

In the middle of the XXIst century, more than half of the existing nuclear facilities around the world are already scheduled for a definitive shut down and the launch of a long deconstruction period. For the majority of them, an important part of the initial phase of in-situ radiological characterization will be performed under several constraints, such as those in difficult access spaces (e.g., embedded piping, ducts, etc.) and the ones with the presence of high radiation levels or even other hazards [4]. Obviously, such constraints condition the measurement instruments to be used, not only from the point of view of the detector or its associated electronics, but also regarding the implementation of accompanying equipment and accessories.

This situation implies the need for targeted criteria allowing the selection of the most appropriate equipment for each situation, taking into account not only the parameter to be determined, but also any radiological and/or non-radiological restriction that may exist in the area where the in-situ measurements should be performed. To do this, it is convenient to analyse the most important characteristics of the equipment that are currently being used, from the most conventional to those that are still being developed or optimized, with emphasis on their response to the restrictive conditions under which such a measurement will be carried out. This is one of the objectives of this paper.

* Corresponding author.
E-mail address: m.herranz@ehu.eus (M. Herranz).

The simplest, fastest and inexpensive NDA technique is that consisting of environmental radiation monitoring at predefined locations to map the associated spatial distribution over vast areas [5]. It is very convenient in the first instance, as it gives an idea about radioactive singularities or hotspots, and can be roughly correlated with the activities of the predominant gamma emitting radionuclides, or the neutron ones on rare occasions. Nevertheless, despite being widely applied, it is seriously affected by substantial uncertainties of the characteristics of the detector used, of the geometric configuration of the whole scene under study, and of the specific properties (frequently not fully known) of the measured objects. Furthermore, cartography of alpha/beta contamination on large surfaces would also be of great utility [6].

Other sophisticated methods, which are able to be applied for the same purpose, are gamma spectrometry, passive neutron counting, and radiation cameras [7—15]. Some of them, although being less used today, still have a great potential, especially if certain challenges, described in the following sections, are addressed.

In those situations when facing the above-mentioned constraints, robotics or other remotely deployed systems based on reduced-size detectors are a good alternative. However, in others, collimation mechanisms with small opening angles may also be considered to restrict the field-of-view of the chosen instruments to only specific portions of the item to be measured. At that stage, the acquisition is then performed at different positions around the object providing a high degree of precision with regard to the spatial distribution of the radioactive source term [16].

The present paper reports on the state-of-the-art of the NDA techniques that can be used for in-situ radiological characterization of nuclear facilities subject to a decommissioning programme. For the sake of clarity and coherence, they have been classified as environmental radiation monitoring, surface contamination measurements, gamma spectrometry, passive neutron counting and radiation cameras. Particular mention is also made here to the various challenges that each of these techniques must currently overcome, together with the formulation of some proposals for a potential evolution in the future. Although some basic concepts are assumed, the interested reader can refer to Refs. [11,17,18] for more details on the theories and practices of radiation instrumentation and detection.

2. Environmental radiation monitoring

At any nuclear facility, environmental radiation monitoring is generally conducted at different positions around its structures in order to investigate their radiological status, to evaluate the effectiveness of protection measures, as well as to assess the associated doses likely to be received by individuals. Depending on the information provided, the measurement techniques used in this domain can be classified into the following three groups: gross counters, air-kerma monitors and probes measuring the ambient dose equivalent or *H*∗(10).

2.1. Gross counting

Gross counting instruments are primarily used to detect the presence of radioactive material. At least in theory, almost any type of the available radiation detectors [11] could be used for this purpose. The oldest one, but still used today, is the Geiger-Müller (GM) counter, which has the advantages of being cheap and robust with a large variety of sizes and it requires minimal electronic processing. It consists of a gas-filled tube whose walls are either metal or have their inner surface coated with a conducting material to operate as a cathode, whereas the anode is made of a wire

mounted axially in the centre of the tube. By applying a polarizing potential difference of several hundred volts, every ionizing particle reaching the detection volume is able to produce a detectable electronic "*pulse*" or "*count*" through both the gas multiplication and electron avalanche mechanisms. In addition, there is a possibility of using GM counters with halogen quenching that helps to maintain their operating lifetime against sustained exposure [19].

However, as all the GM generated pulses almost have the same height, regardless of the number of original electron-ion pairs that initiated the process, these detectors cannot distinguish between radiation types or energies. At best, for a single photon energy, the total count rate (i.e., number of pulses per unit time) will respond linearly with the intensity of the radiation beam. Conversely, for many nuclear facilities, the presence of several radioactive sources emitting X- or γ-rays at various energies might result in erroneous and unreliable interpretation of the measurement results. Instead, thin silicon diodes can also constitute a good alternative due to their radiation hardness and charge collection efficiency [20].

2.2. Air-kerma dosimetry

Kerma represents the amount of the kinetic energies per unit mass of all charged particles initially released by indirectly ionizing or uncharged radiation in a sample of matter. It is quite often confused with the absorbed dose in this industrial sector, as both quantities are expressed in joule per kilogram or Gray (Gy). In the case of photons in air, such a quantity can be measured by an ionization chamber consisting of a gas-filled tube at atmospheric pressure but operating at a very low electric field strength, contrary to a GM counter, to avoid both the gas multiplication and electron avalanche mechanisms.

In such a circumstance, when an incident photon interacts with the gas molecules it may produce electron-ion pairs along its path. The generated ions then drift to the cathode under the influence of the electric field whilst free electrons are collected by the anode and the resulting current remains constant over a given range of the applied voltage.

Yet, ionization chambers used as air-kerma monitors cannot discriminate between radiation types and cannot provide the corresponding energy spectrum. Their wall material is normally selected to have an effective atomic number similar to that of air (Z_{eff} = 7 according to Tahmasebi Birgani et al. [21]). This "*air equivalent*" material has the effect of ensuring that the whole detector is acting as an infinite air volume to reach an electronic equilibrium.

Another alternative to measure air-kerma is the one based on the energy-compensated silicon diodes [22]. Compared to air, these detectors have the inherent advantages of a low ionisation energy and high atomic density, thus allowing very small-sized detectors to be used for routine survey in nuclear facilities.

2.3. H∗(10) dosimetry

The ambient dose equivalent is an imaginary quantity commonly used for monitoring strongly penetrating ionizing radiation, such photons above 12 keV and neutrons [23], as a proxy of the effective dose, which in turn can never be measured in realistic situations because it requires knowledge of the doses delivered to all organs and tissues in the human body.

2.3.1. The case of X- or γ-rays

According to ICRP Publication 74 [24], the ambient dose equivalent in the case of X- and γ-rays is very conservative from the radiation protection point of view since it generally overestimates the effective dose to around 15%—50% in the energy range of 60 keV

to 2 MeV. However, it can even exceed a factor 2 for low energy photons.

Practically any type of photon detector is able to measure $H*(10)$, but the chosen measurement instrument needs to be properly calibrated using standard radioactive sources (most often ^{137}Cs).

2.3.2. The case of neutrons

Although it is not often frequent, measurement of neutrons can provide highly relevant supplementary information, such as before dismantling uranium enrichment plants or the spent fuel reprocessing ones. This should nonetheless consider the fact that neutrons often have fairly wide energy spectra covering, at the same time, a total of 10 decades ranging from 1 meV to several MeV and, as being electrically uncharged, they do not interact with the atomic electrons. The sole way to detect them is through the secondary charged particles released from their varied nuclear interactions in the considered medium. Accordingly, the neutron detection imperatively needs the addition of a converter material offering a significant interaction probability to produce this desired ionization process. The most commonly used are ^3He, ^6Li or ^{10}B due to their optimum cross-section for thermal neutrons (i.e., with energies below 1 eV), as shown in Fig. 1.

To detect more energetic neutrons the conjunct detector + converter is habitually surrounded by an extra moderating material, made of polyethylene, so that their energy is previously slowed down via multiple and/or successive elastic collisions with Hydrogen nuclei. In many instances, further refinements are needed in terms of associated electronics to differentiate between the neutron-induced pulses from those that may be generated by the gamma radiation. Table 1 summarizes the strengths and weaknesses of the most common neutron detectors.

Nevertheless, independently of the considered configuration regarding the detector itself, the converter material and the moderator, satisfactory results in terms of the neutron ambient dose equivalent are only obtained in restricted energy intervals and/or in specific irradiation conditions. Therefore, the chosen instrument must be previously calibrated under the same experimental configurations, or at least considering a representative neutron spectrum [25].

Another option to properly estimate $H*(10)$ would be the preliminary determination of the spectrometric information about all the possible neutron fields in order to derive the proper transfer functions for each location. Among several complex neutron spectrometry techniques, only the Bonner sphere system [26] is able to measure neutron spectra, independently of their direction of incidence, over the whole energy range of interest (i.e., 10^{-3} eV – 10 MeV). The system consists of a set of polyethylene multi-sphere moderators of various sizes (between 2 and 12 inches) surrounding a central detector that is mainly sensitive to thermal neutrons. As the size of the sphere increases, the maximum response of the sphere-detector combination shifts to the highest neutron energies [27]. To derive the spectral contribution of thermal neutrons, an additional measurement must be performed by directly using the central detector in bare configuration or by adding a thin cadmium shell to the smallest polyethylene sphere.

The next crucial challenge in this domain is to design a unique system configuration (detector + converter + moderator) that is suitably optimized regarding its size and weight, preferably with increased radiation tolerance. Such an improvement must allow for real-time measurement of the neutron ambient dose equivalent in every situation, notably referring to their incidence angles and energy distributions, from just a single measurement.

3. Surface contamination measurements

Surface contamination can be *"fixed"* or *"removable"*, depending on whether it can be transferred from a contaminated surface to an uncontaminated one when both accidentally touch. Surface contamination measurements should provide the activity per unit area for all the present radionuclides. Yet, without previous knowledge about the processes behind the presence of these two forms of contamination, it is impossible to make any kind of quantitative assessment about them. As such, only a qualitative
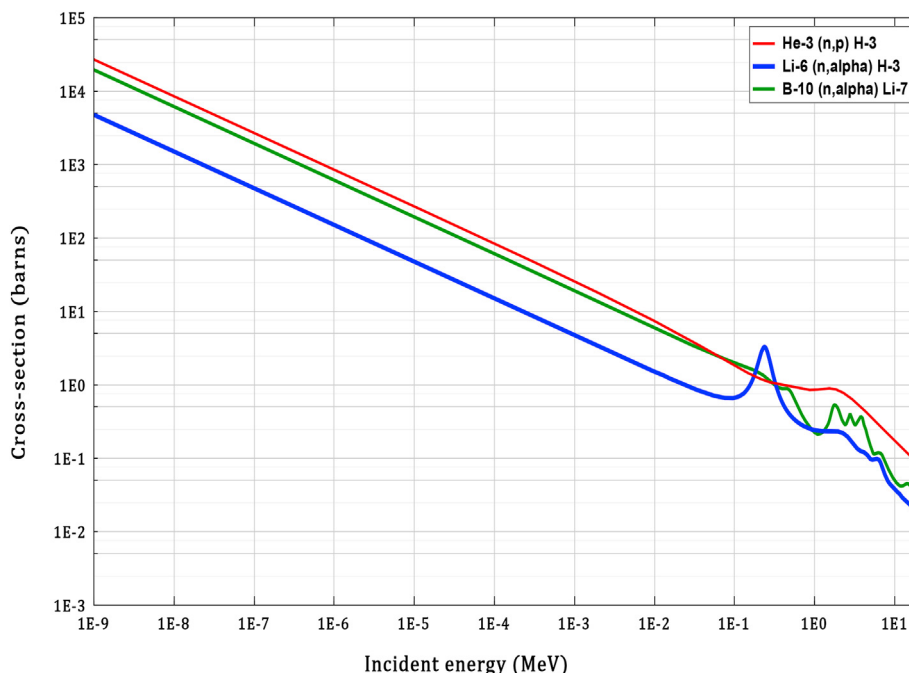

Fig. 1. Cross section vs. incidence energy some nuclear reaction of interest in neutron detection (Source: JANIS, available at: https://www.oecd-nea.org/janis/).

Table 1
Strengths and weaknesses of the most common neutron detectors.

Detector type	Strengths	Weaknesses
^{3}He proportional counter	Reasonably light	Reduced γ pulse discrimination
	Good neutron cross-section	Sensitive to vibrations
	Varied filling pressure	^{3}He shortage
	Resistant to intense radiation fields	
BF$_3$ proportional counter	Reasonably light	Low neutron cross-section
	Good γ rejection	Sensitive to vibrations
	Readily available than ^{3}He	Limited filling pressure
		Toxic and corrosive
LiI(Eu) scintillator	Compact design	Reduced γ pulse discrimination
	Detection efficiency*	Hygroscopic material
	Insensitive to vibrations	Pile-up effect

*: the high atomic density of the crystal fully compensate for the very low cross-section of ^{6}Li.

comparison with clean surfaces and an assessment of which part of the contamination is fixed, and which is removable, can be provided.

In addition, when an exhaustive list of expected radionuclides and their relative contribution to the total activity at a given reference date (commonly called radiological "*fingerprint*") is available, specific calibrations of the measurement instrument are required to achieve reliable quantitative results. Some guides on how to carry out these specific calibrations are already established by the ISO standards 7503 [28–30].

There are two methods to measure radioactive contamination on surfaces: "*directly*" by keeping the radiation detector almost immobile, as close as possible to the surface under examination (no more than a few mm), or "*indirectly*" by means of smear tests. Whereas the direct method can handle both types of surface contamination, the indirect one allows for the evaluation of the corresponding removable part only after wiping the surfaces concerned by this issue. Afterwards, the collected smears can be measured outside of the area being monitored, preferably in another location with low background radiation, and/or sent to a radiochemical laboratory for a more precise analysis.

While carrying out the direct method, special care needs to be taken to avoid contamination of the detector itself. In addition, such a method must be applied on accessible, smooth and even surfaces that are ideally free from solid or liquid deposits. If any of these conditions is not met or if there is an excessive level of interfering radiation, the indirect method should be considered, even though it cannot properly assess fixed contamination and has a high degree of uncertainty, given the lack of knowledge regarding the effectiveness of the wiping.

Table 2 provides an overview of the strengths and weaknesses of each method. The two methods are often complementary and together they help to provide a comprehensive picture of the contamination state of the studied zone.

Proportional counters could measure the radioactive contamination on surfaces directly, since they have a small dead time effect and can enable discriminating the alpha-induced pulses from the beta ones [31]. They consist of gas-filled tubes operating in a voltage region immediately after that of an ionization chamber. Consequently, the electric field strength is intense enough to accelerate the primary free electrons, which are released after each interaction of the incident radiation, to energies so high that their collisions with the gas molecules cause further ionizations before reaching the anode. This effect, called gas multiplication, makes the height of the output electric pulse proportional to the energy deposited by the incident radiation. The detection volume can be fully sealed after the gas filling or can operate under a continuous flow [32], which is quite impractical or entirely unfeasible in the majority of in-situ applications.

Other types of detectors like plastic scintillators [33,34] also represent a highly effective alternative, mainly due to their ability to differentiate between various types of radiation and to provide the corresponding spectrometric information. An interesting issue for further development in this field would be the implementation of an automatic measurement instrument that is able to gather accurate real-time data, unequivocally with regard to both identification and quantification, about practically any kind of mixture of pure beta and/or alpha emitting radionuclides likely to be present on contaminated surfaces.

3.1. Alpha contamination

Because of the extremely low penetration of alpha particles, an appropriate barrier must be implemented to let them come into contact with the sensitive region of a detector, while simultaneously protecting this latter, *inter alia*, against inner contamination. Most times, a detector with an ultra-thin (~0.8 mg/cm^2) end-window, made of an aluminized mylar or mica film, is used, and thus any eventual contact with hard objects may puncture it. This can cause a gas exhaust when using a proportional counter or the entrance of ambient light to sensitive crystal in the case of scintillators detectors, hence overwhelming the photomultiplier tube.

3.2. Beta contamination

Many of the problems encountered during the measurement of alpha contamination do not apply for β-particles, except perhaps for those with a low penetrating power like ^{3}H, ^{63}Ni and ^{241}Pu. Notwithstanding, as most of the conventional detectors used are also sensitive to X/γ-rays, they cannot systematically assess the

Table 2
Overview of the strengths and weaknesses of surface contamination measurements depending on the method used.

Method type	Strengths	Weaknesses
Direct	Total contamination measurement	Not suitable on all surfaces
	Control of large areas	Sensitivity to high radiation background
Indirect	Very simple concept	Wiping effectiveness
	Access to loose contamination	Fixed contamination representability

individual contribution of each radiation. This issue is normally solved by making an additional measurement with a filter thick enough to only absorb the incident β-particles, thus enabling the estimation of the background contribution to the detector reading.

4. Gamma spectrometry

Gamma spectrometry is the start NDA technique, as some radionuclides of interest emit characteristic X- and/or γ-rays with specific energies, intensities and decay probabilities, hence allowing their identification and quantification. Its general principle consists in measuring one or more of these mono-energetic photons with a detector that is able to generate a pulse signal, the height of which is proportional to the amount of energy deposited within the sensitive volume. This energy transmission can be either total or partial, depending on the different interaction mechanisms (photoelectric, Compton scattering and pair production) followed by each incident photon. The usage of a multi-channel analyser (MCA) and evaluation algorithm is henceforth recommended for a proper display of the recorded pulse-height histogram.

The following two key parameters must be considered when performing a γ-spectrometry:

- the energy resolution, indicating the ability of the detector to distinguish between incident photons with very close energies, and
- the absolute efficiency of detection, which is universally defined as the number of net pulses under the observed full-energy peak, often called "*photopeak*", divided by the number of its associated X- or γ-rays emitted by the radioactive source.

Indeed, this last parameter varies depending on the detector type, the emission energy, the geometric configuration (measurement distances, use of collimation, shielding, screens, etc.), as well as the corresponding self-absorption effect in the measured item. A complete characterisation of the detector response is normally carried out by means of radioactive standard sources and theoretical calculations [35–37].

It should be emphasised, moreover, that energy resolution is also paramount when trying to measure low activity X- or γ-emitting radionuclides in the presence of background and Compton interference. In fact, the higher the energy resolution of a given detector, the better its signal-to-noise ratio [38].

When projecting gamma spectrometry for in-situ radiological characterization, the net count rates under the observed photopeaks must at last be converted into activity concentrations of the associated radionuclides, taking into account several plausible hypotheses regarding the volume distribution of the radioactive source term within the object under examination. For this purpose, as nuclear facilities contain huge and complex equipment, ad hoc transfer functions need to be calculated on a case-by-case basis from a theoretical model representing the physical characteristics of the object itself (shape, volume, weight or mass density and material composition), the different distances scheduled for measurements, and all the possible volume distributions of the sought radionuclides.

The gamma spectrometers most commonly employed in this industrial sector are based on inorganic scintillators, such as NaI(Tl), LaBr or BGO, as well as on high-purity germanium (HPGe), CdTe or CdZnTe semiconductors. Their typical energy resolutions with respect to ^{57}Co (122 keV) and ^{137}Cs (662 keV) peaks are given in Table 3.

All these spectrometers, described below, are usually used under an open geometry, also known as "*one shot*" measurement, with the shielded detector located in a fixed position and rightly

Table 3
Typical energy resolution for different gamma spectrometers.

Energy	NaI(Tl)	LaBr	BGO	CZT	CdTe	HPGe
122 keV	~15 keV	~8 keV	~30 keV	~8 keV	~2 keV	~0.5 keV
662 keV	~46 keV	~20 keV	~66 keV	~17 keV	~4 keV	~1.0 keV

oriented so that its field-of-view allows to "*see*" the whole volume of the item to be measured [39]. However, the corresponding results are generally more sensitive to the variations of the radioactivity distribution within objects and their matrix effect. A collimation mechanism with a small opening angle can then be added to the detector to reduce the associated uncertainties.

4.1. Scintillation detectors

Scintillation is the emission of a flash of light in transparent materials when exposed to an ionizing radiation. A scintillation detector consists of a scintillator crystal (NaI(Tl), CsI, SrI$_2$, LiI, LiF, LaBr, LaCl$_3$, CeBr$_3$, BGO, etc.) coupled with an electronic light sensor, which is traditionally a photomultiplier tube (PMT). The latter converts every light photon emitted by the scintillator into an electrical pulse that provides a meaningful information about the energy deposited by the incident radiation.

Scintillation detectors can be manufactured in large volumes but they generally have poor energy resolution. They are therefore often employed for low-level radioactivity measurements with simple X/γ spectra. However, since most scintillators have a very fast signal response, they can likewise be applied at high count rates or for coincidence counting.

As they are the most representative of all the above-mentioned scintillator crystals used for gamma spectrometry, only NaI(Tl), LaBr and BGO are described in the following subsections. The big challenge for this family of detectors is to obtain a new scintillation material that offers an enhanced energy resolution while preserving, as much as possible, other relevant parameters, such as response linearity, fast pulse rise/fall time, nearly symmetric peaks, thermal stability, absence of internal radioactivity, radiation resistance, etc.

4.1.1. NaI(Tl)

Sodium iodide crystal activated with thallium or NaI(Tl) is the classical scintillation crystal, available in a large variety of sizes and geometries, and its detection efficiency has been historically taken as the reference for the other γ-spectrometers. Its energy resolution is nonetheless very limited (see Table 3), it does not tolerate high radiation levels [40] and it is a hygroscopic material. Consequently, it cannot tolerate exposition to humid environments and requires the use of a hermetically sealed assembly, but with a minimum front-end thickness so as not to hinder the detection efficiency at low energies. The detector encapsulation is often made from low atomic number metal or metal alloys (e.g., aluminium). An additional aspect that must be highlighted is its complex response behaviour (in terms of light output, energy resolution and decay time constant) at varied ambient temperatures [41].

4.1.2. LaBr

Cerium-doped lanthanum bromide or LaBr$_3$(Ce), often abbreviated as LaBr, is one of the promising new generation of scintillation detectors, offering improved energy resolution (see Table 3), slightly better detection efficiency and fast emission rates compared to NaI(Tl). It is also a hygroscopic material that needs a protective encapsulation, but with an adequate temperature tolerance [42] and a good resistance to intense radiation fields [40].

Although the LaBr crystals are currently available in small sizes, they are very appropriate to be applied in spaces with limited accessibility, especially when coupled with silicon drift detectors (SDD) or silicon photomultipliers (SiPM).

4.1.3. BGO

Bismuth germanium oxide or BGO, which can be manufactured under different chemical compositions [43], is a relatively hard, rugged and non-hygroscopic crystal, so no particular hermetic sealing is required. Although its light output is only 10 to 15% that of NaI(Tl), it is considered to have a superior detection efficiency given its high density, almost twice that of NaI(Tl), and atomic number, which definitely enhances photoelectric interactions of incident X- and/or γ-rays and the their associated peak-to-total ratios. However, it has a very limited energy resolution and does not tolerate temperature variations.

4.2. Semiconductor detectors

In semiconductor detectors, ionizing radiation is measured by the number of charge carriers (i.e., electrons and holes) set free after its interaction with the substrate material, which is arranged between two electrodes. Under the influence of an electric field, the number of collected charge carriers when exposed to an ionizing radiation results in a pulse signal that is significantly lower than in scintillation detectors, but with better energy resolution.

It must be noted that semiconductor detectors are relatively sensitive to performance degradation when exposed to intense radiation fields, especially in the case of neutrons. Electronic components are also radiation-sensitive, particularly the pre-amplifiers, which are the first stage in the signal processing chain for both the scintillators and semiconductors.

Among the available semiconductors, only the most common ones will be described in the following subsections, namely HPGe, CdTe and CZT. The first of them has an excellent energy resolution but low detection efficiency and it needs reinforced cooling to cryogenic temperature (<120 K) given its narrow band gap [44]. The other two, in spite of being able to operate at room temperature, have good detection efficiencies but not optimum energy resolutions. The ultimate goal for this type of detectors continues to be the achievement of an energy resolution quite similar to that of HPGe but at ambient temperatures.

4.2.1. HPGe

The operating principle of germanium detectors is fully based on that of a *p-n* junction, which is a transition zone, depleted of charge carriers, created in the contact between a *n*-type semiconductor (with excess electron concentration) and a *p*-type semiconductor (with excess hole concentration) from the same crystal. This junction behaves like a diode, allowing the electric current to flow in a unique direction and can be made wide enough, under a reverse-bias voltage (i.e., in the direction of no electric current flow), to enable the detection of both X- and γ-rays.

However, unwanted impurities in the crystal material trap electrons and holes that may be generated by the incident radiation, ruining the performance of the detector, so purification techniques should be applied. High-purity Germanium (HPGe) detectors are characterised by an excellent energy resolution. In addition, they may have large sensitive volumes, ranging from cm^3 to about 1 L, which can be used as total absorption detectors for photon energies up to several MeV.

Their major drawback is that the crystal must be placed in a vacuum cryostat and cooled to cryogenic temperatures, which may restrict their usefulness in a number of in-situ applications, namely in zones with limited accessibility or with radioactive contamination. In these two cases, an HPGe detector coupled with a compact pulse-tube cryocooler [45] is to be considered among other refrigeration options.

In environments where the electronics can be damaged by the circumstances (e.g., intense radiation fields), it is possible to use a low-noise charge preamplifier allowing the remote control of the detector with adequate shielding from large distances [46].

4.2.2. CdTe or CZT

The main advantage of the Cadmium telluride (CdTe) or cadmium zinc telluride (CdZnTe or CZT) crystals, when compared to that of HPGe, is their high detection efficiency because of their high atomic number and density, thus favouring photoelectric interactions. Moreover, their wide band gap allows them to operate in room temperatures (i.e., from −5 °C to 50 °C according to Park et al. [47]) without requiring reinforced cooling.

Their energy resolution is not as optimal as that of HPGe detectors, but it is slightly better than that of scintillators. In contrast, they are characterized by a poor mobility for both electrons and holes due to the charge trapping effect that is mainly caused by structural defects, impurities and other irregularities (e.g., dislocations, inclusions, etc.). This usually results in the so-called low-energy tailing of the observed peaks in the measured spectrum, which needs to be accounted for during data processing.

CdTe and CZT detectors are generally fabricated with *ohmic* or *Schottky* contacts, allowing measurements over a wide range of radiation dose rates between 10 μGy/h and 100 mGy/h. The corresponding radiation-induced damage has been investigated by Cavallini et al. [48], demonstrating that CdTe is quite insensitive to an integrated ^{60}Co gamma dose up to 10 kGy, whereas CZT starts degrading only after 25 kGy irradiation. According to the same authors, exposition above this value causes a full degradation of its spectroscopic capabilities, such as a loss of energy resolution and an incomplete charge collection.

5. Passive neutron counting

Passive neutron counting is an exclusive NDA technique that is able to deliver relevant information about the presence of fissile materials after a detailed analysis of the spontaneous neutrons principally emitted by the plutonium isotopes: ^{238}Pu, ^{240}Pu and ^{242}Pu [17]. Its main advantage is its low dependence regarding dense objects containing such radioactive elements. Compared to gamma spectrometry, it is less sensitive to metallic matrices, commonly found in nuclear facilities, making these two techniques quite complementary. Of course, it also has its own limitations that will be discussed in this section.

For many years, a set of ^3He proportional counters, duly arranged in the shape of long tubes inside a polyethylene block, has been the preferred measuring system in this domain. However, because of the acute shortage of this rare non-radioactive gas, some serious alternatives have been or are being explored [49–61].

There are two modes of passive neutron counting. In the total mode, all the incident neutrons are measured, without distinction between their emission process, that is spontaneous fission or (α,n) reactions. Whereas in the coincidence mode, we only record the number of times that time-correlated neutrons (pairs, triplets or even more) issued from spontaneous fission are detected. With either these two counting modes, the presence of neutron absorbers or other materials rich in hydrogen, like water, plastics and paraffin, may reduce the signals of interest.

Another important limitation of the total counting mode is its high dependence with regard to the chemical form of the plutonium isotopes, consisting essentially of pure metal, PuO_2 and PuF_4 [17]. In addition, any potential presence of other α-emitting

radionuclides, which cannot be completely ruled out, may equally generate neutrons via (α,n) reactions that are expected to happen with most light elements, from lithium up to chlorine.

Unfortunately, all the energy spectra originally emitted from the aforementioned neutron sources, independently of the production mechanism that is followed, are broad enough to cover the entire range between 0.1 and 10 MeV without showing any substantial difference between them [25]. Therefore, the direct identification of a given neutron-emitting radionuclide through its energy spectrum is not at all feasible.

Anyhow, this difficulty can be overcome by analysing the temporal dynamics of all the recorded signals and discriminating between events issued from spontaneous fission and those resulting from (α,n) reactions. This would thus facilitate the quantification of the number of the coincident neutrons, which do not depend in any way on the chemical form of the plutonium isotopes. Such an information is subsequently used to estimate the masse of fissile materials in terms of effective ^{240}Pu mass that would give the same coincidence response as the measured one.

Notwithstanding, neutron coincidence counting has the disadvantage of being extremely affected by the ^{242}Cm and ^{244}Cm spontaneous neutron emission, which is very intense, representing a factor between 4170 and 20600 times higher than for the plutonium isotopes [17].

In all circumstances, detailed information concerning the presence of actinides in the source term, and on the isotopic composition of the sought fissile materials, would be of great help in order to better interpret the measurement results. This information could be based on previous inventories, though preliminary, and/or from further gamma spectrometry. Otherwise, a complete sensitivity study needs to be carried out, by means of theoretical calculations and different statistical deconvolution methods, considering all realistic hypothesis and evaluating their impact on the measurement uncertainties. The whole characterization of the chosen measurement instrument is usually conducted considering standard neutron sources (e.g., ^{241}Am–Be and ^{252}Cf), as well as numerical simulations using MCNPX [62] or other Monte Carlo codes [63–65].

At the risk of being repetitive, the same challenge stated in Section 2.3.2 is also valid for total neutron counting. In the case of coincidence mode, there have certainly been many recent efforts to build transportable and easy-to-handle systems [66] but their cost remains prohibitive.

6. Radiation cameras

Radiation cameras may provide another valuable solution that cannot be disregarded for in-situ radiological characterization of nuclear facilities subject to a decommissioning programme. Their associated information regarding the relative intensity of the ionizing radiation being measured (i.e., a sort of colour map display) is directly superimposed on the real view of the scene under study, normally taken by a visible camera. Hence, they allow for the localisation of radioactive objects or hotspots from greater distances than conventional instruments, thus significantly reducing the radiation dose received by operators in line with the ALARA (*as low as reasonably achievable*) principle [67].

The deployment of this type of equipment requires coupling with other instruments or acquisition methods: vision, telemetry, gamma spectrometry, etc. These additional systems should collect at least dimensional data (position of the probe in space), identification of radionuclides, radiation levels, and/or a visible image. Today, modules often associated with a robotized platform or drones grouping several instruments [68–75] could be deployed to surmount many of the constraints encountered in nuclear facilities [4].

6.1. Gamma cameras

Current γ-cameras are undergoing impressive developments in terms of lightness, compactness, usability, response sensitivity, angular resolution, panoramic vision and spectrometric capabilities. According to their measurement principle, they can be classified into three categories: Compton, pinhole and coded aperture. In what follows, we introduce the main concepts of each of these techniques, whose main strengths and weaknesses are summarized in Table 4. This section ends with a rough description of the stereo γ-camera, which represents the latest technological breakthrough that has been developed very recently [76].

6.1.1. Pinhole technique

A pinhole photographic camera, also known as "*dark chamber*", is a simple optical imaging device in the shape of a light-opaque box. On one of its sides is a small aperture through which the light coming from an outside source is projected as an inverted image on the opposite side inside the box. Initially, this technique was applied for different purposes until the mid-20th century when scientists discovered that it could also be used to visualise gamma sources [77]. Nevertheless, the pinhole size has a direct impact on its angular resolution and signal-to-noise ratio (SNR). The smaller the aperture diameter, the better the angular resolution, but the poorer the signal-to-noise ratio. Therefore, a compromise must be reached with respect to these two performance parameters.

An earlier attempt to develop a portable gamma camera based on the pinhole technique was carried out in the 1990s by CEA [10]. This instrument is a mature technology combining an inverted double-cone collimator (i.e., two right circular cones placed apex-to-apex) to be used as a single pinhole aperture, a CsI/Tl (thallium doped caesium iodide) scintillation crystal, a multi-channel image intensifier, and a CCD camera. With the exception of the pinhole aperture, the whole instrument is fully shielded against background radiation (see Fig. 2), leading to a very narrow collimation angle. There is also the possibility of taking an extra measurement in every situation by placing a dense screen or shutter over the pinhole aperture to have a "*blank*" image, the correction of which hence allows improving the signal-to-noise ratio.

In short, the shielding requirement could be suitable for high dose rate environments, like that currently encountered inside the reactor containment vessels of the Fukushima Daiichi nuclear power plant [78]. It however poses several restrictions from the practical point of view, due to the heavy weight of the instrument in question, as well as the lowest amount of incident photons allowed through such a small frond-end opening. In order to improve all these aspects, the implementation of a coded aperture technique was first tested by the Kurchatov Institute [79] and then by CEA [80].

6.1.2. Coded aperture technique

The principle of a coded aperture mask is the use of a front-end collimator with several pinholes defined by a given rank and thickness in mm. The motivation behind this design was to preserve many of the pinhole properties, like its high angular resolution, while significantly improving the signal-to-noise ratio of the acquired images, proportionally to the sum of the open areas of all the pinholes constituting the coded aperture mask [81].

For an accurate localisation of radioactive sources, a coded aperture mask based on the Modified Uniformly Redundant Array or MURA [82] is placed in front of a pixelated detector, as illustrated in Fig. 3. The photon beam coming from any γ-emitting source is modulated by the coded aperture mask and projected on the pixelated detector surface as a shadow image. To obtain the

Table 4
Strengths and weaknesses of the different γ-camera types.

| Detector type	Strengths	Weaknesses
Pinhole	Optimal angular resolution (1.9°−6.7°)	Heavy (≥15 kg)
	Wide energy range (from[241]Am to[60]Co)	Low sensitivity (~0.5 μSv/h[137]Cs in 10 min)
	Good dose-rate linearity	Small field-of-view (30° or 50°)
	Enhanced signal-to-noise ratio	Moderate energy resolution
Coded aperture	Can be ultra-compact (<300 g)	Small field-of-view (45°−50°)
	High sensitivity (~2 nSv/h[241]Am in 2 min)	Moderate energy resolution
	Optimal angular resolution (2.5°−6°)	
	Wide energy range (from 30 keV to[60]Co)	
	Dose-rate linearity up to 10 Sv/h	
Compton	Can be compact (3−5 kg)	Low sensitivity (30 nSv/h[137]Cs in 5 min)
	Field-of-view up to 360°	Moderate angular resolution (10°−30°)
	High energy resolution (~1% at 662 keV)	Hardly applicable below 250 keV
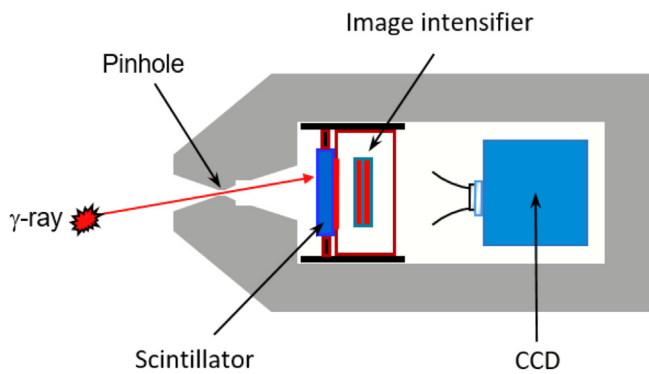
Fig. 2. Illustration of the pinhole γ-camera concept.

position of the source with respect to the γ-camera field-of-view, the reconstruction technique described by Gottesman & Fenimore [82] is adopted.

As explained by Braga et al. [83], an important limitation of such a reconstruction technique is the systematics arising from the non-uniform detector spatial response. Furthermore, in the correlation process, any variation in the background level measured by different segments of the detector plane can affect the estimates of source intensities. A solution to these problems is to observe the source field in alternate measurements: the mask pattern can be inverted by a 90° rotation [84]. Such rotation creates an anti-mask of the original pattern, except for the central element. This provides an anti-mask measurement without additional weight and complex mechanical manipulations. By performing alternate measurements with a mask and with an anti-mask for equal time

durations, the systematic effects are eliminated. The main features and performances of existing ultra-portable and compact γ-cameras based on the coded aperture technique have been extensively studied as reported in Refs. [7,85,86], although the latter reference is rather focused on medical applications.

Relying on all the above capabilities, a new automatic method has been proposed to obtain panoramic views of both optical and radiation images based on a robust homography estimation [87]. This method allows self-locating radioactive sources or hotspots that would potentially exceed the field-of-view of the camera while preserving their geometrical coherency. Moreover, the feasibility of analysing large rooms or facilities has been proved by displaying the respective results within a single image, enabling the rendering of spherical images and the creation of interactive virtual tours.

6.1.3. Compton technique

Compton cameras consider inelastic photon scattering theory to reconstruct the location of radioactive sources [88,89]. They typically consist of two parallel and energy sensitive detectors (see Fig. 4). When an incident γ-ray with energy E_0 hits the camera, it may undergo Compton scattering in the first detector, called "*scatter*" detector, and photoelectric absorption in the second one, called "*absorber*" detector. Let E_1 and E_2 be the energies as measured by these two detectors, respectively, we should then have $E_0 = E_1 + E_2$. By quoting the positions of each interaction and applying the laws of conservation of energy and momentum in physics, the scattering angle θ is obtained as follows:

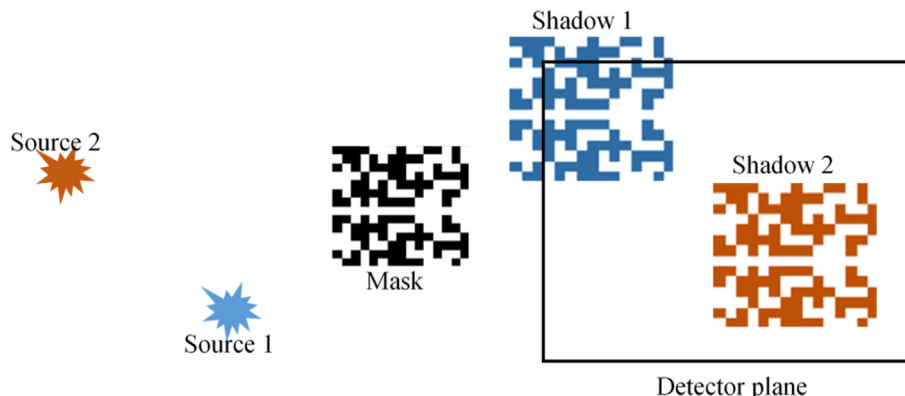$$\cos\theta = 1 - m_e c^2 \left(\frac{1}{E_2} - \frac{1}{E_1 + E_2} \right)$$

Fig. 3. Illustration of the coded aperture concept for two radioactive sources placed at different locations within the field-of-view of the γ-camera.
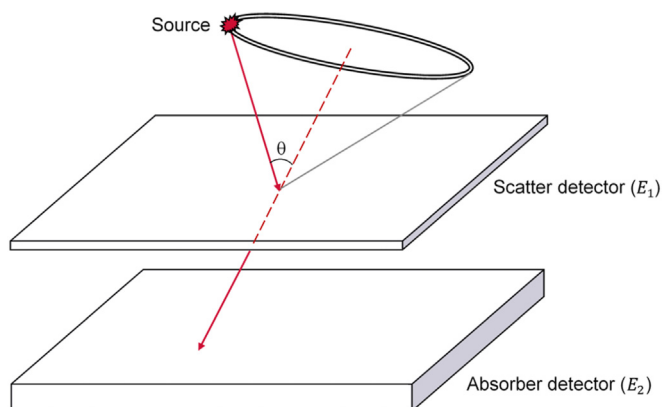
Fig. 4. Illustration of the Compton γ-camera concept, where E_1 and E_2 are the energies as measured by the scatter detector and the absorber one, respectively.

where m_e is the electron rest mass and c is the speed of light in vacuum.

The photon origin can thus be constrained to the surface of a back-projected cone, called the *Compton cone*, spanned by θ with its apex given by the primary interaction position in the scatter detector. From the intersection of different Compton cones, inferred from subsequent photons susceptible to generate coincident interaction events (scattering followed by a photoelectric absorption) in both detectors, the location of the corresponding emitting source can be determined.

According to Table 4, Compton γ-cameras present an optimal field-of-view (up to 360°) and a high-energy resolution (~1% for the ^{137}Cs 662 keV γ-rays) when compared to both pinhole and coded aperture techniques. Conversely, they have a very limited angular resolution (10°−30°), they are hardly applicable below 250 keV and they are less sensitive, as only a small portion of incident γ-rays can generate the signals of interest in the two detectors.

As an example of field-testing of such an interesting technique under real conditions, several measurements have been conducted inside the turbine building of Unit 3 of the Fukushima Daiichi nuclear power plant and made it possible to locate all the radioactive hotspots [90]. They have also allowed visualizing a high-dose spatial distribution map (up to 3.5 mSv/h) of the studied environment after integrating the associated point cloud data provided by a laser rangefinder. The same technique was also successfully used by Wahl et al. [91] inside the residual-heat-removal pump room at a given US nuclear facility (they did not specify where exactly). The authors were thus able to detect and identify the presence of two cobalt isotopes (^{58}Co and ^{60}Co) in different portions of the pump, as well as a known ^{137}Cs contamination on the floor and the wall behind the camera, issued from a past flood of the room. Afterwards, the camera was oriented towards two pipes in the room to determine which of them was radioactive in order to foresee some shielding. It however showed that almost all the radioactivity came from a third pipe under the floor, which was unexpected before. By placing protective material on the floor, it was therefore possible to significantly reduce the dose to workers. Such a radiological protection was not anticipated from previous conventional measurements.

Over the last few years, there have also been fairly promising initiatives to develop hybrid γ-cameras by combining all the advantages of the Compton technique either with the coded aperture ones [92] or with those of an active pinhole [93].

6.1.4. Stereo gamma camera

The existing industrial γ-cameras only provide a planar or two-dimensional (2-D) view showing the presence of radiation emitting objects in the surrounding environment. That is, they just superimpose a colour map display, indicating the amount of the emitted γ-rays, on the optical image of the scene under study, but without the possibility of determining the distance between the located radioactive sources and the measuring instrument.

The adoption of both gamma and optical sensors also leads to significant parallax errors between the respective acquired images, which is often manually corrected by assigning the average source-to-detector distance. However, such a correction though presents several problems. Overall, the superimposition can be coherently performed only if the person using the γ-camera already knows which object is supposed to be radioactive. However, this fact might limit the benefit of using γ-cameras, as the radioactivity location is not always known a priori. An alternative type of scenario that might occur is when several radioactive sources are detected at different locations within the field-of-view of the γ-camera, making it impossible to infer a unique distance for all of them. Indeed, even if we successfully correct by hand the parallax error on one of these sources, the others will not be properly superimposed, thus leading to potentially misleading results.

To overcome this difficulty, a stereo γ-camera has been recently developed [76] to localise radioactive sources, regardless of their shape and volume, even when they are behind an occluding object (e.g., wall) or covered by other materials (e.g., within a barrel) without being fully shielded. This is a straightforward technique able to directly extract both visible and gamma 3-D information of a scene, by applying a triangulation approach from at least two different perspectives, like those obtained by the human eyes (left and right). When applied to two identical γ-cameras, whose detection centres are horizontally separated from each other, such a technique allows to automatically estimate the actual distance to any radiation emitting position within their shared field-of-view through the disparity map [94], computed as pixel-by-pixel shifts between their respective reconstructed images. Values in this disparity map are inversely proportional to the scene depth at the corresponding pixel location. Fig. 5 illustrates the basic concept of a stereo γ-camera in the case of a radioactive point source.

6.2. Alpha cameras

In spite of their short range in air, the remote and safe localisation of materials or surfaces contaminated with α emitters is possible based on the ionization-induced fluorescence of airborne molecules [8]. As shown in Fig. 6, after depositing their energy in a small layer of air, monochromatic ultraviolet (UV) lights are emitted because of the presence of nitrogen, which is the major air component (up to ~ 78%). Such a radiation has quite a long range in air, allowing for direct visualisation of the location of the corresponding pure alpha sources, with the help of an adapted optical camera, preferably with an optimum spectral response in the UV−visible range, and appropriate light filters to easily retrieve both pieces of information. It moreover enables that kind of detection even in the presence of beta and/or gamma radiation, because of their inability to generate as much localized fluorescence as in the case of α-particles, and also through UV transparent materials [95], namely the translucent ones, making it possible to take the complementary visible pictures.

Normally, the camera does not find the exact position of an α-emitting radionuclide, but rather a fluorescence zone around it. As a rough approximation, this zone usually has a spherical shape, with a radius equal to the range of α-particle in air (e.g., ~5 cm for $E_\alpha = 6$ MeV), and is subjected to a fluorescence gradient, being the most intense luminous part highly condensed in its centre, within only few mm from the emission point [12].
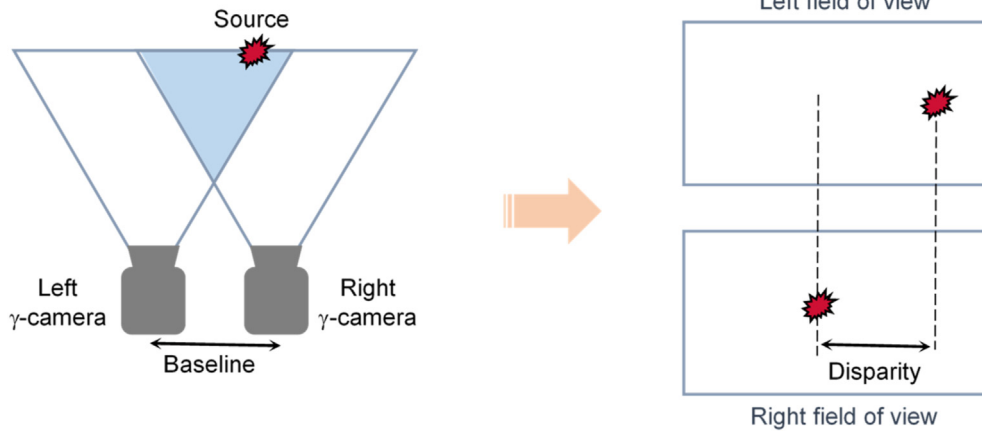
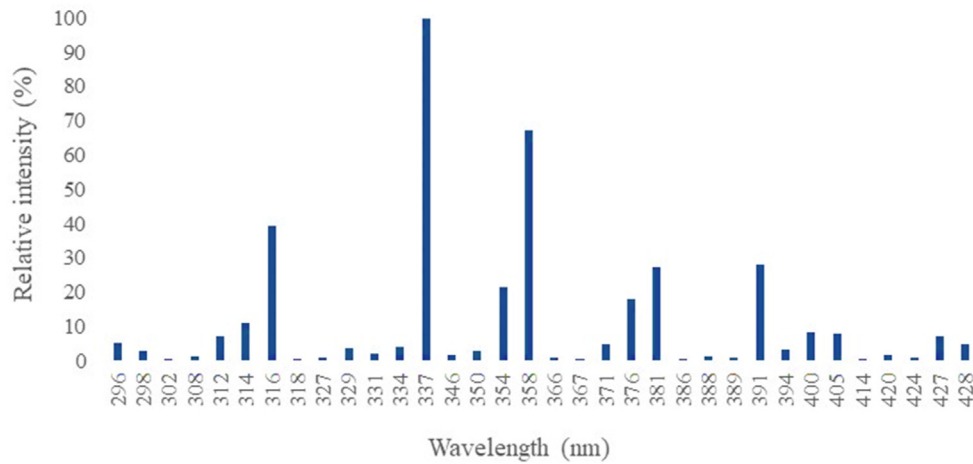**Fig. 5.** Illustration of the stereo γ-camera concept in the case of a radioactive point source.

Fig. 6. Typical UV emission lines of dry air at 800 hPa and 293 K [96].

The UV-fluorescence yield depends on the energy of every α-particle stopped in air, as well as on the ambient temperature, pressure and humidity. According to the experiments carried out by Sand et al. [97], later confirmed through Geant4 predictions [98], it is assumed to be proportional to the absorbed energy and that almost 20 UV photons per MeV can be released in the case of dry air at normal temperature and pressure. The authors have additionally put in evidence the strongest luminescence in pure nitrogen atmospheres (up a factor of 6 times higher than in air) and the quenching effect of water molecules, together with oxygen. Better still, it has been recently shown that when the air is fully purged with nitrogen containing a trace amount (~50 ppm) of nitric oxide (NO), UV-fluorescence can even be up to 150 times more intense, especially at wavelengths between 200 nm and 280 nm [99].

This imaging technique, which was originally employed to observe cosmic ray showers in the Earth's atmosphere in the form of large-aperture telescopes [100], has been optimized since the last decade to develop field-deployable cameras able to search for alpha contamination on surfaces from a sufficient stand-off distance [101–113]. Most of these cameras were tested in realistic fields, providing very encouraging results. This was particularly true, although not exclusively, when the sought α-emitting radionuclides were enclosed within a glove box made of Plexiglass or inside a hot cell with a lead glass window [12,107,111].

Nevertheless, their intrinsic sensitivity must improve to be

likewise applied under natural or artificial lighting conditions. To date, the preferred mitigation measures involve controlling the lighting of the scene or performing measurements in complete darkness. Other improvements consisted of just considering the so-called solar-blind photodiodes with a wavelength cut-off below 280 nm [103,106,108,112] or else taking advantage, where possible, of the recorded spectroscopic information [101]. These are chief aspects needing further efforts to be unquestionably consolidated.

6.3. Neutron cameras

In principle, neutron imaging could also be performed based on both the pinhole and the coded aperture techniques described above [114]. The difference with respect to gamma cameras is the type of materials selected for shielding (e.g., lead or tungsten for γ-rays and borated polyethylene for neutrons). In addition, neutrons may undergo proton recoil scattering that provides analogous directional information, as in the case of the Compton technique that only applies to photons. However, the mathematical expression here is quite different and is derived, by virtue of kinematics, from the recoil proton energy E_p deposited in the first segmented (or position-sensitive) detector and the remaining scattered neutron energy, E_{ns}, which can be measured using the time-of-flight to the second detector, Therefore, the neutron scattering angle is calculated as follows [115]:

$$\tan \theta = \sqrt{E_p / E_{ns}}$$

where $E_n = E_p + E_{ns}$ is the neutron incident energy.

Several prototypes have been recently developed for many applications related to in-situ radiological characterisation, radiation protection of workers, assurance of nuclear non-proliferation safeguards and homeland security, especially those associated with the prevention of illicit trafficking in radioactive materials [14], [116–126]. Others are also able to operate in dual neutron-gamma imaging mode [127–132].

Notwithstanding, the challenge for the in-situ radiological characterisation of nuclear facilities to be dismantled, is still to design neutron cameras that are as compact and robust as possible, demanding less logistical arrangements, while remaining sufficiently sensitive to neutrons and optimizing their angular resolution. Potentially, Lynde et al. [133] and Whitney et al. [134] each proposed a good compromise in this aspect.

7. Conclusions and perspectives

This paper gives a review of the main non-destructive techniques usually used for in-situ radiological characterisation of nuclear facilities subject to a decommissioning programme. Broadly speaking, the important thing to retain here is that there is no universal solution, as the choice of the appropriate techniques depends on the characterization objectives and on the potential constraints under which the measurement must be performed. Accordingly, the most widespread techniques until now generally consist of environmental radiation monitoring, surface contamination measurements, gamma spectrometry, passive neutron counting, and radiation cameras.

For the two first techniques providing preliminary screening information, several existing instruments and methodologies are applied because of their robustness and fitness to meet pre-established purposes. Potential further developments in this domain could be the miniaturization of the most common devices along with their components and the implementation of an automatic measurement probe able to gather accurate real-time data, unequivocally with respect to both identification and quantification, about practically any kind of mixture of pure beta and/or alpha emitting radionuclides likely to be present on contaminated surfaces.

Regarding gamma-spectrometry, there is a general agreement that high-purity germanium (HPGe) is the favourite detector due to its excellent energy resolution. However, the fact that it must operate under reinforced cooling to cryogenic temperature may restrict its usefulness to a number of in-situ applications, namely in zones with limited accessibility. Great efforts must therefore be exerted to obtain a new gamma spectrometer, whether based on a scintillation detector or on a semiconductor one, offering the optimum energy resolution at room temperature while preserving, as much as possible, other relevant parameters, such as response linearity, fast pulse rise/fall time, nearly symmetric peaks, thermal stability, absence of internal radioactivity, radiation resistance, etc.

The next crucial challenge when measuring neutrons is to design a unique system configuration (detector + converter + moderator) that is suitably optimized regarding its size and weight, preferably with increased radiation tolerance. Such an improvement must allow for real-time measurement of the neutron ambient dose equivalent in any situation, notably referring to their incidence angles and energy distributions, from just a single measurement. In the case of neutron coincidence counting, there have certainly been many recent efforts to develop transportable and easy-to-handle systems, but their cost remains prohibitive.

Finally, concerning radiation cameras, where more developments are strongly emerging, the possibility of evolving towards a multifunctional, highly compact and fully autonomous instrument, which guarantees the localisation of radioactive sources, independently of whether they are emitting gammas, alphas or neutrons, would be very beneficial for the majority of nuclear installations.

Declaration of Competing Interest

The authors declare that they have no known competing financial interests or personal relationships that could have appeared to influence the work reported in this paper.

Acknowledgements

References

[1] International Atomic Energy Agency, IAEA Safety Glossary: 2018 Edition, 2019. Vienna.

[2] Nuclear Energy Agency, Organisation for Economic Co-Operation and Development, R&D and Innovation Needs for Decommissioning Nuclear Facilities, 2014. Report No. 7191.

[3] International Atomic Energy Agency, Radiological Characterization of Shut Down Nuclear Reactors for Decommissioning Purposes, Technical Report Series No. 389, 1998. Vienna.

[4] F. Aspe, R. Idoeta, G. Auge, M. Herranz, Classification and categorization of the constrained environments in nuclear/radiological installations under decommissioning and dismantling processes, Prog. Nucl. Energy 124 (2020) 102247.

[5] S. Mikami, T. Maeyama, Y. Hoshide, R. Sakamoto, S. Sato, N. Okuda, T. Sato, H. Takemiya, K. Saito, The air dose rate around the Fukushima Dai-ichi Nuclear Power Plant: its spatial characteristics and temporal changes until December 2012, J. Environ. Radioact. 139 (2015) 250–259.

[6] R. Haudebourg, P. Fichet, A non-destructive and on-site digital autoradiography-based tool to identify contaminating radionuclide in nuclear wastes and facilities to be dismantled, J. Radioanal. Nucl. Chem. 309 (2016) 551–561.

[7] K. Amgarou, V. Paradiso, A. Patoz, F. Bonnet, J. Handley, P. Couturier, F. Becker, N. Menaa, A comprehensive experimental characterization of the iPIX gamma imager, J. Instrum. 11 (2016) P08012.

[8] S.M. Baschenko, Remote optical detection of alpha particle sources, J. Radiol. Prot. 24 (2004) 75–82.

[9] M.J. Cieślak, K.A.A. Gamage, R. Glover, Coded-aperture imaging systems: past, present and future development − A review, Radiat. Meas. 92 (2016) 59–71.

[10] O. Gal, C. Izac, F. Lainé, A. Nguyen, CARTOGAM: a portable gamma camera, Nucl. Instrum. Methods A 387 (1997) 297–303.

[11] G.F. Knoll, Radiation Detection and Measurement, fourth ed., John Wiley & Sons, 2010.

[12] F. Lamadie, F. Delmas, C. Mahé, P. Gironès, C. Le Goaller, J.R. Costes, Remote alpha imaging in nuclear installations: new results and prospects, IEEE Trans. Nucl. Sci. 52 (2005) 3035–3039.

[13] G. Kindleben, R. Baumann, Decommissioning of a MOX fuel fabrication facility: criticality safety aspects, in: Proceedings of the Seventh International Conference on Nuclear Criticality Safety, 2003. Tokai, Ibaraki, Japan, October 20-24.

[14] R.S. Woolf, B.F. Phlips, A.L. Hutcheson, E.A. Wulf, Fast-neutron, coded-aperture imager, Nucl. Instrum. Methods A 784 (2015) 398–404.

[15] S. Takeda, Y. Ichinohe, K. Hagino, H. Odaka, T. Yuasa, S. Ikelshikawa, T. Fukuyama, S. Saito, T. Sato, G. Sato, S. Watanabe, M. Kokubun, T. Takahashi, M. Yamaguchi, H. Tajima, T. Tanaka, K. Nakazawa, Y. Fukazawa, T. Nakano, Applications and imaging techniques of a Si/CdTe Compton gamma-ray camera, Phys. Procedia 37 (2012) 859–866.

[16] B.A. Cattle, A.S. Fellerman, R.M. West, On the detection of solid deposits using gamma ray emission tomography with limited data, Meas. Sci. Technol. 15 (2004) 1429–1439.

[17] D. Reilly, N. Ensslin, H. Jr Smith, Passive Non-destructive Assay of Nuclear Materials, Los Alamos National Laboratory, 1991. NUREG/CR-5550/LA-UR-90-732.

[18] N. Tsoulfanidis, S. Lansberger, Measurement and Detection of Radiation, fourth ed., CRC Press, 2015.

[19] M. Abilama, M. Bates, A. Lohstroh, Investigating the lifetime of bromine-quenched G.M. Counters with temperature, Nucl. Instrum. Methods A 795 (2015) 12–18.

[20] M. Boscardin, M. Bruzzi, A. Candelori, G.-F.D. Betta, E. Focardi, V. Khomenkov, C. Piemonte, S. Ronchin, C. Tosi, N. Zorzi, Radiation hardness and charge collection efficiency of lithium irradiated thin silicon diodes, IEEE Trans. Nucl. Sci. 52 (2005) 1048–1053.

[21] M.J. Tahmasebi Birgani, F. Seif, N. Chegeni, M.R. Bayatiani, Determination of the effective atomic and mass numbers for mixture and compound materials in high energy photon interactions, J. Radioanal. Nucl. Chem. 292 (2012) 367–1370.

[22] Ü. Ören, L. Herrnsdorf, M. Gunnarsson, S. Mattsson, C.L. Rääf, Can an energy-compensated solid-state x-ray detector be used for radiation protection applications at higher photon energies? Radiat. Protect. Dosim. 169 (2016) 292–296.

[23] International Commission on Radiation Units and Measurements, Quantities and unit in radiation protection dosimetry, ICRU (Int. Comm. Radiat. Units Meas.) Rep. 51 (1993).

[24] International Commission on Radiological Protection, Conversion coefficients for use in radiological protection against external radiation, ICRP (Int. Comm. Radiol. Prot.) Publ. 74 (1996).

[25] International Atomic Energy Agency, Compendium of Neutron Spectra and Detector Responses for Radiation Protection Purposes, Supplement to Technical Reports Series No. 318, 2001. Vienna.

[26] R.L. Bramblett, R.I. Ewing, T.W. Bonner, A new type of neutron spectrometer, Nucl. Instrum. Methods 9 (1960) 1–12.

[27] K. Amgarou, V. Lacoste, Response matrix evaluations of a passive Bonner sphere system used for neutron spectrometry at pulsed, intense and complex mixed fields, J. Instrum. 5 (2010) P09002.

[28] International Organization for Standardization, Measurement of Radioactivity – Measurement and Evaluation of Surface Contamination – Part 1: General Principles, June 2017. NF ISO 7503-1.

[29] International Organization for Standardization, Measurement of Radioactivity – Measurement and Evaluation of Surface Contamination – Part 2: Test Method Using Wipe-Test Samples, June 2017. NF ISO 7503-2.

[30] International Organization for Standardization, Measurement of Radioactivity – Measurement and Evaluation of Surface Contamination – Part 3: Apparatus Calibration, June 2017. NF ISO 7503-3.

[31] P.H. Burgess, Handbook on Measurement Methods and Strategies at Very Low Levels and Activities, European Commission, Nuclear Safety and the Environment, 1998. Report EUR 17624.

[32] X. Tuo, K. Mu, Z. Li, X. Li, Tritium monitor based on gas-flow proportional counter, J. Nucl. Sci. Technol. 45 (2008) 171–174.

[33] Y. Morishita, K. Hoshi, T. Torii, Evaluation of an ultra-thin plastic scintillator to detect alpha and beta particle contamination, Nucl. Instrum. Methods A 966 (2020) 163795.

[34] J. Venara, M. Ben Mosbah, C. Mahé, J. Astier, S. Adera, M. Cuozzo, V. Goudeau, Design and development of a portable β-spectrometer for 90Sr activity measurements in contaminated matrices, Nucl. Instrum. Methods A 953 (2020) 163081.

[35] J. Boson, G. Ågren, L. Johansson, A detailed investigation of HPGe detector response for improved Monte Carlo efficiency calculations, Nucl. Instrum. Methods A 587 (2008) 304–314.

[36] D. Sahin, K. Ünlü, Modeling a gamma spectroscopy system and predicting spectra with Geant-4, J. Radioanal. Nucl. Chem. 282 (2009) 167–172.

[37] R. Venkataraman, F. Bronson, V. Atrashkevich, M. Field, B.M. Young, Improved detector response characterization method in ISOCS and LabSOCS, J. Radioanal. Nucl. Chem. 264 (2005) 213–219.

[38] G.A. Armantrout, A.E. Bradley, P.L. Phelps, Sensitivity problems in biological and environmental counting, IEEE Trans. Nucl. Sci. 19 (1972) 107–116.

[39] International Organization for Standardization, Guidance for Gamma Spectrometry Measurement of Radioactive Waste, NF EN ISO 19017, October 2017.

[40] S. Normand, A. Iltis, F. Bernard, T. Domenech, P. Delacour, Resistance to γ irradiation of LaBr3:Ce and LaCl3:Ce single crystals, Nucl. Instrum. Methods A 572 (2006) 754–759.

[41] M. Moszynski, A. Nassalski, A. Syntfeld-Kazuch, T. Szczensniak, W. Czarnacki, D. Wolski, G. Pausch, J. Stein, Temperature dependences of LaBr3(Ce), LaCl3(Ce) and NaI(Tl) scintillators, Nucl. Instrum. Methods A 588 (2006) 739–751.

[42] G. Bizarri, J.T.M. de Haas, P. Dorenbos, C.W.E. van Eijk, Scintillation properties of Ø 1×1 inch^3 LaBr$_3$: 5%Ce^{3+} crystal, IEEE Trans. Nucl. Sci. 53 (2006) 615–619.

[43] H.O. Tekin, L.R.P. Kassab, S.A.M. Issa, M.M. Martins, L. Bontempo, G.R. da Silva Mattos, Newly developed BGO glasses: synthesis, optical and nuclear radiation shielding properties, Ceram. Int. 46 (2020) 11861–11873.

[44] D.L. Upp, R.M. Keyser, T.R. Twomey, New cooling methods for HPGE detectors and associated electronics, J. Radioanal. Nucl. Chem. 264 (2005) 121–126.

[45] P.E. Tissot, L. Crowe, J. Colvin, T.L. Mann, A. Guerra, Design and testing of a pulse tube based cooling system for high purity germanium detectors, in: P. Kittel (Ed.), Advances in Cryogenic Engineering, vol. 43, Springer, Boston, MA, 1998.

[46] A. Pullia, F. Zocca, C. Cattadori, Single-transistor option for high-resolution γ-ray spectroscopy in hostile environments, IEEE Nucl. Sc. Symp. Conf. Rec.

[47] S.H. Park, J.H. Ha, J.H. Lee, H.S. Kim, Y.H. Cho, S.D. Cheon, D.G. Hong, Effect of temperature on the performance of a CZT radiation detector, J. Kor. Phys. Soc. 56 (2010) 1079–1082.

[48] A. Cavallini, B. Fraboni, N. Auricchio, E. Caroli, W. Dusi, P. Chirco, M.P. Morigi, M. Zanarini, M. Hage-Ali, P. Siffert, P. Fougeres, Irradiation-induced defects in CdTe and CdZnTe detectors, Nucl. Instrum. Methods A 458 (2001) 392–399.

[49] J.S. Beaumont, T.H. Lee, M. Mayorov, A fast-neutron coincidence collar using liquid scintillators for fresh fuel verification, J. Radioanal. Nucl. Chem. 314 (2017) 803–812.

[50] C. Cowles, S. Behling, P. Baldez, M. Folsom, R. Kouzes, V. Kukharev, A. Lintereur, S. Robinson, E. Siciliano, S. Stave, P. Valdez, Development of a lithium fluoride zinc sulfide based neutron multiplicity counter, Nucl. Instrum. Methods A 887 (2018) 59–63.

[51] A. Di Fulvio, T.H. Shin, T. Jordan, C. Sosa, M.L. Ruch, S.D. Clarke, D.L. Chichester, S.A. Pozzi, Passive assay of plutonium metal plates using a fast-neutron multiplicity counter, Nucl. Instrum. Methods A 855 (2017) 92–101.

[52] C. Eleon, F. Battiston, M. Bounaud, M. Ben Mosbah, C. Passard, B. Perot, Boron-coated straws imaging panel capability for passive and active neutron measurements of radioactive waste drums, IEEE Trans. Nucl. Sci. 67 (2020) 2096–2104.

[53] M.J. Joyce, K.A.A. Gamage, M.D. Aspinall, F.D. Cave, A. Lavietes, Real-time, fast neutron coincidence assay of plutonium with a 4-channel multiplexed analyzer and organic scintillators, IEEE Trans. Nucl. Sci. 61 (2014) 1340–1348.

[54] R.T. Kouzes, J.H. Ely, A.T. Lintereur, E.R. Siciliano, Boron-10 based neutron coincidence counter for safeguards, IEEE Trans. Nucl. Sci. 61 (2014) 2608–2618.

[55] R.T. Kouzes, A.T. Lintereur, E.R. Siciliano, Progress in alternative neutron detection to address the helium-3 shortage, Nucl. Instrum. Methods A 784 (2015) 172–175.

[56] H.O. Menlove, S.H. Menlove, S.J. Tobin, Fissile and fertile nuclear material measurements using a new differential die-away self-interrogation technique, Nucl. Instrum. Methods A 602 (2009) 588–593.

[57] A. Ocherashvili, E. Roesgen, A. Beck, E.N. Caspi, M. Mosconi, J.-M. Crochemore, B. Pedersen, SNM detection by means of thermal neutron interrogation and a liquid scintillation detector, J. Instrum. 7 (2012) C03037.

[58] H.M.O. Parker, J.S. Beaumont, M.J. Joyce, Passive, non-intrusive assay of depleted uranium, J. Hazard Mater. 364 (2019) 293–299.

[59] G.C. Rich, K. Kazkaz, H.P. Martinez, T. Gushue, Fabrication and characterization of a lithium-glass-based composite neutron detector, Nucl. Instrum. Methods A 794 (2015) 15–24.

[60] B. Simony, B. Pérot, C. Carasco, F. Jallu, N. Saurel, S. Colas, P. Gironès, J. Collot, Passive neutron coincidence counting with plastic scintillators for the characterization of radioactive waste drums, IEEE Trans. Nucl. Sci. 64 (2017) 2719–2724.

[61] S. Stave, M. Bliss, R. Kouzes, A. Lintereur, S. Robinson, E. Siciliano, L. Wood, LiF/ZnS neutron multiplicity counter, Nucl. Instrum. Methods A 784 (2015) 208–212.

[62] D.B. Pelowitz, MCNPX^{TM} User's Manual, Version 2.7.0, Los Alamos National Laboratory, 2011. LA-CP-11-00438.

[63] S. Agostinelli, J. Allison, K. Amako, J. Apostolakis, H. Araujo, P. Arce, M. Asai, D. Axen, S. Banerjee, G. Barrand, F. Behner, L. Bellagamba, J. Boudreau, L. Broglia, A. Brunengo, H. Burkhardt, S. Chauvie, J. Chuma, R. Chytracek, G. Cooperman, G. Cosmo, P. Degtyarenko, A. Dell'Acqua, G. Depaola, D. Dietrich, R. Enami, A. Feliciello, C. Ferguson, H. Fesefeldt, G. Folger, F. Foppiano, A. Forti, S. Garelli, S. Giani, R. Giannitrapani, D. Gibin, J.J. Gómez Cadenas, I. González, G. Gracia Abril, G. Greeniaus, W. Greiner, V. Grichine, A. Grossheim, S. Guatelli, P. Gumplinger, R. Hamatsu, K. Hashimoto, H. Hasui, A. Heikkinen, A. Howard, V. Ivanchenko, A. Johnson, F.W. Jones, J. Kallenbach, N. Kanaya, M. Kawabata, Y. Kawabata, M. Kawaguti, S. Kelner, P. Kent, A. Kimura, T. Kodama, R. Kokoulin, M. Kossov, H. Kurashige, E. Lamanna, T. Lampén, V. Lara, V. Lefebure, F. Lei, M. Liendl, W. Lockman, F. Longo, S. Magni, M. Maire, E. Medernach, K. Minamimoto, P. Mora de Freitas, Y. Morita, K. Murakami, M. Nagamatu, R. Nartallo, P. Nieminen, T. Nishimura, K. Ohtsubo, M. Okamura, S. O'Neale, Y. Oohata, K. Paech, J. Perl, A. Pfeiffer, M.G. Pia, F. Ranjard, A. Rybin, S. Sadilov, E. Di Salvo, G. Santin, T. Sasaki, N. Savvas, Y. Sawada, S. Scherer, S. Sei, V. Sirotenko, D. Smith, N. Starkov, H. Stoecker, J. Sulkimo, M. Takahata, S. Tanaka, E. Tcherniaev, E. Safai Tehrani, M. Tropeano, P. Truscott, H. Uno, L. Urban, P. Urban, M. Verderi, A. Walkden, W. Wander, H. Weber, J.P. Wellisch, T. Wenaus, D.C. Williams, D. Wright, T. Yamada, H. Yoshida, D. Zschiesche, Geant4—a simulation toolkit, Nucl. Instrum. Methods A 506 (2003) 250–303.

[64] E. Brun, F. Damian, C.M. Diop, E. Dumonteil, F.X. Hugot, C. Jouanne, Y.K. Lee, F. Malvagi, A. Mazzolo, O. Petit, J.C. Trama, T. Visonneau, A. Zoia, Tripoli-4®, CEA, EDF and AREVA reference Monte Carlo code, Ann. Nucl. Energy 82 (2015) 151–160.

[65] A Ferrari, P.R. Sala, A. Fasso, J. Ranft, FLUKA: a Multi-Particle Transport Code, CERN-2005-10, INFN/TC_05/11, SLAC-R-773.

[66] R. Rossa, A. Borella, S. Boden, W. Broeckx, Estimation of fissile material content in irradiated In-Pile Sections using neutron coincidence counters, EPJ Web Conf. 225 (2020), 06001.

[67] International Commission on Radiological Protection, 2007 Recommendations of the International Commission on Radiological Protection, vol. 103,

ICRP Publication, 2007.

[68] H. Ardiny, S. Witwicki, F. Mondada, Autonomous exploration for radioactive hotspots localization taking account of sensor limitations, Sensors 19 (2019) 292.

[69] C. Ducros, G. Hauser, N. Mahjoubi, P. Girones, L. Boisset, A. Sorin, E. Jonquet, J.M. Falciola, A. Benhamou, RICA: a tracked robot for sampling and radiological characterization in the nuclear field, J. Field Robot. 34 (2017) 583–599.

[70] M. Gianni, Towards expendable robot teaming in extreme environments, Int. J. Mech. Eng. Robot. Res. 8 (2019) 830–838.

[71] D. Hellfeld, P. Barton, D. Gunter, A. Haefner, L. Mihailescu, K. Vetter, Real-time free-moving active coded mask 3d gamma-ray imaging, IEEE Trans. Nucl. Sci. 66 (2019) 2252–2260.

[72] S. Mochizuki, J. Kataoka, L. Tagawa, Y. Iwamoto, H. Okochi, N. Katsumi, S. Kinno, M. Arimoto, T. Maruhashi, K. Fujieda, T. Kurihara, S. Ohsuka, First demonstration of aerial gamma-ray imaging using drone for prompt radiation survey in Fukushima, J. Instrum. 12 (2017) P11014.

[73] I. Tsitsimpelis, C.J. Taylor, B. Lennox, M.J. Joyce, A review of ground-based robotic systems for the characterization of nuclear environments, Prog. Nucl. Energy 111 (2019) 109–124.

[74] Y. Ueno, I. Takahashi, T. Ishitsu, T. Tadokoro, K. Okada, Y. Nagumo, Y. Fujishima, Y. Kometani, Y. Suzuki, K. Umegaki, Spectroscopic gamma camera for use in high dose environments, Nucl. Instrum. Methods A 822 (2016) 48–56.

[75] K. Vetter, R. Barnowski, J.W. Cates, A. Haefner, T.H. Joshi, R. Pavlovsky, B.J. Quiter, Advances in nuclear radiation sensing: enabling 3-D gamma-ray vision, Sensors 19 (2019) 2541.

[76] V. Paradiso, K. Amgarou, N. Blanc de Lanaute, F. Bonnet, O. Beltramello, E. Liénard, 3-D localization of radioactive hotspots via portable gamma cameras, Nucl. Instrum. Methods A 910 (2018) 194–203.

[77] R.K. Mortimer, H.O. Anger, C.A. Tobias, The Gamma-Ray Pinhole Camera with Image Amplifier, U.S. Atomic Energy Commission, University of California Radiation Laboratory, 1954. UCRL-2524.

[78] K. Sueoka, J. Kataoka, M. Takebe, Y. Iwamoto, M. Arimoto, M. Yoneyama, I. Yoda, T. Torii, Y. Sato, M. Kaburagi, Y. Terasaka, Development of a new pinhole camera for imaging in high dose-rate environments, Nucl. Instrum. Methods A 912 (2018) 115–118.

[79] O.P. Ivanov, A.N. Sudarkin, V.E. Stepanov, L.I. Urutskoev, Portable X-ray and gamma-ray imager with coded mask: performance characteristics and methods of image reconstruction, Nucl. Instrum. Methods A 422 (1999) 729–734.

[80] O. Gal, M. Gmar, O.P. Ivanov, F. Lainé, F. Lamadie, C. Le Goaller, C. Mahé, E. Manach, V.E. Stepanov, Development of a portable gamma camera with coded aperture, Nucl. Instrum. Methods A 563 (2006) 233–237.

[81] E. Caroli, J.B. Stephen, G. Di Cocco, L. Natalucci, A. Spizzichino, Coded aperture imaging in X- and gamma-ray astronomy, Space Sci. Rev. 45 (1987) 349–403.

[82] S.R. Gottesman, E.E. Fenimore, New family of binary arrays for coded aperture imaging, Appl. Opt. 28 (1989) 4344–4352.

[83] J. Braga, T. Villela, U.B. Jayanthi, F. D'Amico, J.A. Neri, A new mask-antimask coded-aperture telescope for hard x-ray astronomy, Exp. Astron. 2 (1991) 101–113.

[84] S. Sun, Y. Liu, X. Ouyang, Near-field high-resolution coded aperture gamma-ray imaging with separable masks, Nucl. Instrum. Methods A 951 (2020) 163001.

[85] G. Amoyal, V. Schoepff, F. Carrel, V. Lourenco, D. Lacour, T. Branger, Metrological characterization of the GAMPIX gamma camera, Nucl. Instrum. Methods A 944 (2019) 162568.

[86] P. Russo, F. Di Lillo, V. Corvino, P.M. Frallicciardi, A. Sarno, G. Mettivier, CdTe compact gamma camera for coded aperture imaging in radioguided surgery, Phys. Med. 69 (2020) 223–232.

[87] V. Paradiso, K. Amgarou, N. Blanc de Lanaute, V. Schoepff, G. Amoyal, C. Mahé, O. Beltramello, E. Liénard, A panoramic coded aperture gamma camera for radioactive hotspots localization, J. Instrum. 12 (2017) P11010.

[88] Y.F. Du, Z. He, G.F. Knoll, D.K. Wehe, W. Li, Evaluation of a Compton scattering camera using 3-D position sensitive CdZnTe detectors, Nucl. Instrum. Methods A 457 (2001) 203–211.

[89] M. Frandes, B. Timar, D. Lungeanu, Image reconstruction techniques for Compton scattering based imaging: an overview, Curr. Med. Imag. Rev. 12 (2016) 95–105.

[90] Y. Sato, Y. Tanifuji, Y. Terasaka, H. Usami, M. Kaburagi, K. Kawabata, W. Utsugi, H. Kikuchi, S. Takahira, T. Torii, Radiation imaging using a compact Compton camera inside the Fukushima Daiichi nuclear power station building, J. Nucl. Sci. Technol. 55 (2018) 965–970.

[91] C.G. Wahl, W.R. Kaye, W. Wang, F. Zhang, J.M. Jaworski, A. King, Y.A. Boucher, Z. He, The Polaris-H imaging spectrometer, Nucl. Instrum. Methods A 784 (2015) 377–381.

[92] G. Amoyal, V. Schoepff, F. Carrel, M. Michel, N. Blanc de Lanaute, J.C. Angélique, Development of a hybrid gamma camera based on Timepix3 for nuclear industry applications, Nucl. Instrum. Methods A 987 (2021) 164838.

[93] A. Omata, J. Kataoka, K. Fujieda, S. Sato, E. Kuriyama, H. Kato, A. Toyoshima, T. Teramoto, K. Ooe, Y. Liu, K. Matsunaga, T. Kamiya, T. Watabe, E. Shimosegawa, J. Hatazawa, Performance demonstration of a hybrid Compton camera with an active pinhole for wide-band X-ray and gamma-ray imaging, Sci. Rep. 10 (2020) 14064.

[94] D. Marr, T. Poggio, Cooperative computation of stereo disparity, Science 194 (1976) 283–287.

[95] J. Feener, W. Charlton, Preliminary results of nuclear fluorescence imaging of alpha and beta emitting sources, in: Proceedings of the 3rd International Conference on Advancements in Nuclear Instrumentation Measurement Methods and Their Applications (ANIMMA), France, 2013. Marseille.

[96] M. Ave, M. Bohacova, B. Buonomo, N. Busca, L. Cazon, S.D. Chemerisov, M.E. Conde, R.A. Crowell, P. Di Carlo, C. Di Giulio, M. Doubrava, A. Esposito, P. Facal, F.J. Franchini, J. Hörandel, M. Hrabovsky, M. Iarlori, T.E. Kasprzyk, B. Keilhauer, H. Klages, M. Kleifges, S. Kuhlmann, G. Mazzitelli, L. Nozka, A. Obermeier, M. Palatka, S. Petrera, P. Privitera, J. Ridky, V. Rizi, G. Rodriguez, F. Salamida, P. Schovanek, H. Spinka, E. Strazzeri, A. Ulrich, Z.M. Yusof, V. Vacek, P. Valente, V. Verzi, T. Waldenmaier, Measurement of the pressure dependence of air fluorescence emission induced by electrons, Astropart. Phys. 28 (2007) 41–57.

[97] J. Sand, S. Ihantola, K. Peräjärvi, H. Toivonen, J. Toivonen, Radioluminescence yield of alpha particles in air, New J. Phys. 16 (2014), 053022.

[98] C.I. Thompson, E.E. Barritt, C. Shenton-Taylor, Predicting the air fluorescence yield of radioactive sources, Radiat. Meas. 88 (2016) 48–54.

[99] T. Kerst, J. Toivonen, Intense radioluminescence of NO/N2-mixture in solar blind spectral region, Opt Express 26 (2018) 33764–33771.

[100] F. Arqueros, J.R. Hörandel, B. Keilhauer, Air fluorescence relevant for cosmic-ray detection—summary of the 5th fluorescence workshop, El Escorial 2007, Nucl. Instrum. Methods A 597 (2008) 1–22.

[101] J. Brett, K.E. Koehler, M. Bischak, J. Famiano, J. Jenkins, L. Klankowski, P. Niraula, P. Pancella, R. Lakis, Spectral measurements of alpha-induced radioluminescence in various gases, Nucl. Instrum. Methods A 184 (2017) 88–93.

[102] D. Chichester, S. Watson, Multispectral UV-visual imaging as a tool for locating and assessing ionizing radiation in air, IEEE Trans. Nucl. Sci. 58 (2011) 2512–2518.

[103] A.J. Crompton, K.A.A. Gamage, S. Bell, A.P. Wilson, A. Jenkins, D. Trivedi, First results of using a UVtron flame sensor to detect alpha-induced air fluorescence in the UVC wavelength range, Sensors 17 (2017) 2756.

[104] S. Ihantola, J. Sand, K. Peräjärvi, J. Toivonen, H. Toivonen, Fluorescence-assisted gamma spectrometry for surface contamination analysis, IEEE Trans. Nucl. Sci. 60 (2013) 305–309.

[105] O. Ivanov, A. Danilovich, V. Stepanov, S. Smirnov, A. Volkovich, Visualization of radioactive rources without gamma-radiation with UV imaging systems, in: Proceedings of the ASME 2009 12th International Conference on Environmental Remediation and Radioactive Waste Management, 2009. Liverpool, UK.

[106] O.P. Ivanov, V.E. Stepanov, S.V. Smirnov, A.G. Volkovich, Development of method for detection of alpha contamination with using UV-camera "DayCor" by OFIL, IEEE Nucl. Sci. Symp. Conf. Rec. (2011) 2192–2194.

[107] T. Kerst, J. Sand, S. Ihantola, K. Peräjärvi, A. Nicholl, E. Hrnecek, A. Toivonen, J. Toivonen, Standoff alpha radiation detection for hot cell imaging and crime scene investigation, Opt. Rev. 25 (2018) 429–436.

[108] F.S. Krasniqi, T. Kerst, M. Leino, J.-T. Eisheh, H. Toivonen, A. Röttger, J. Toivonen, Standoff UV-C imaging of alpha particle emitters, Nucl. Instrum. Methods A 987 (2021) 164821.

[109] N. Kume, K. Takakura, K. Nakayama, H. Kuroda, M. Izumi, N. Mukai, Remote detector of alpha-ray using ultraviolet ray emitted by nitrogen in air, in: IEEE Nuclear Science Symposium and Medical Imaging Conference (2013 NSS/MIC), 2013. Seoul, South Korea.

[110] C. Mahé, Alpha imaging: recent achievements and glove box characterization, in: Proceedings of the Decommissioning, Decontamination, and Reutilization Topical Meeting, Idaho Falls, ID, USA, 2010.

[111] J. Sand, S. Ihantola, K. Peräjärvi, A. Nicholl, E. Hrnecek, H. Toivonen, J. Toivonen, Imaging of alpha emitters in a field environment, Nucl. Instrum. Methods A 782 (2015) 13–19.

[112] J. Sand, A. Nicholl, E. Hrnecek, H. Toivonen, J. Toivonen, K. Peräjärvi, Stand-off radoluminescence mapping of alpha emitters under bright lighting, IEEE Trans. Nucl. Sci. 63 (2016) 1777–1783.

[113] J. Yao, J. Brenizer, R. Hui, S. Yin, Standoff alpha radiation detection via excited state absorption of air, Appl. Phys. Lett. 102 (2013) 254101.

[114] P.E. Vanier, Analogies between Neutron and Gamma-Ray Imaging, Brookhaven National Laboratory, BNL-76974-2006-CP, 2006.

[115] P.E. Vanier, L. Forman, I. Dioszegi, C. Salwen, V.J. Ghosh, Calibration and testing of a large-area fast-neutron directional detector, IEEE Nucl. Sci. Symp. Conf. Rec. (2007) 179–184.

[116] J. Brennan, E. Brubaker, M. Gerling, P. Marleau, K. McMillan, A. Nowack, N. Renard-Le Galloudec, M. Sweany, Demonstration of two-dimensional time-encoded imaging of fast neutrons, Nucl. Instrum. Methods A 802 (2015) 76–81.

[117] J.E.M. Goldsmith, M.D. Gerling, J.S. Brennan, A compact neutron scatter camera for field deployment, Rev. Sci. Instrum. 87 (2016), 083307.

[118] C.V. Griffith, R.S. Woolf, B.F. Phlips, 64-element fast-neutron, coded-aperture imager, IEEE International Symposium on Technologies for Homeland Security (HST), Waltham, MA, USA, 2017.

[119] P.A. Hausladen, M.A. Blackston, R.J. Newby, Position-sensitive Fast-Neutron Detector Development in Support of Fuel-Cycle R&D MPACT Campaign, Oak Ridge National Laboratory, 2010. ORNL/TM-2010/201.

[120] P. Hausladen, J. Newby, F. Liang, M. Blackston, A Deployable Fast-Neutron

Coded-Aperture Imager for Quantifying Nuclear Material, Oak Ridge National Laboratory, 2013. ORNL/TM-2013/248.

[121] P. Hausladen, J. Newby, F. Liang, M. Blackston, The Deployable Fast-Neutron Coded-Aperture Imager: Demonstration of Locating One or More Sources in Three Dimensions, Oak Ridge National Laboratory, 2013. ORNL/TM-2013/446.

[122] M.G. Makowska, B. Walfort, A. Zeller, C. Grünzweig, T. Bücherl, Performance of the commercial PP/ZnS:Cu and PP/ZnS:Ag scintillation screens for fast neutron imaging, J. Imaging 3 (2017) 60.

[123] X. Pang, Z. Zhang, J. Zhang, W. Zhou, Y. Zhang, D. Cao, L. Shuai, Y. Wang, Y. Liu, X. Jiang, X. Liang, X. Xiao, L. Wei, D. Li, A compact MPPC-based camera for omnidirectional (4π) fast-neutron imaging based on double neutron—proton elastic scattering, Nucl. Instrum. Methods A 944 (2019) 162471.

[124] O.H.W. Siegmund, J.V. Vallerga, A.S. Tremsin, W.B. Feller, High spatial and temporal resolution neutron imaging with microchannel plate detectors, IEEE Trans. Nucl. Sci. 56 (2009) 1203—1209.

[125] Y. Tian, Y. Fu, Y. Li, Y. Li, Development of a 3-D Position Sensitive Neutron Detector Based on Organic Scintillators with Double Side SiPM Readout, in: IEEE Nuclear Science Symposium and Medical Imaging Conference, NSS/MIC, Atlanta, GA, USA, 2017.

[126] K. Weinfurther, J. Mattingly, E. Brubaker, J. Steele, Model-based design evaluation of a compact, high-efficiency neutron scatter camera, Nucl. Instrum. Methods A 883 (2018) 115—135.

[127] H. Al Hamrashdi, D. Cheneler, S.D. Monk, A fast and portable imager for neutron and gamma emitting radionuclides, Nucl. Instrum. Methods A 953 (2020) 163253.

[128] B. Ayaz-Maierhafer, J.P. Hayward, K.P. Ziock, M.A. Blackston, L. Fabris, Transmission and signal loss in mask designs for a dual neutron and gamma imager applied to mobile standoff detection, Nucl. Instrum. Methods A 712 (2013) 1—8.

[129] B. Ayaz-Maierhafer, J.P. Hayward, K.P. Ziock, M.A. Blackston, Angular resolution study of a combined gamma-neutron coded aperture imager for standoff detection, Nucl. Instrum. Methods A 712 (2013) 120—125.

[130] A. Poitrasson-Rivière, M.C. Hamel, J.K. Polack, M. Flaska, S.D. Clarke, S.A. Pozzi, Dual-particle imaging system based on simultaneous detection of photon and neutron collision events, Nucl. Instrum. Methods A 760 (2014) 40—45.

[131] N.P. Shah, J. VanderZanden, D.K. Wehe, Design and construction of a 1-D, cylindrical, dual-particle, time-encoded imaging system, Nucl. Instrum. Methods A 954 (2020) 161785.

[132] R.S. Woolf, B.F. Phlips, A.L. Hutcheson, L.J. Mitchell, E.A. Wulf, An Active Interrogation Detection System (ACTINIDES) Based on a Dual Fast Neutron/gamma-Ray Coded Aperture Imager, IEEE Conference on Technologies for Homeland Security (HST), Waltham, MA, USA, 2012.

[133] C. Lynde, F. Carrel, V. Schoepff, C. Frangville, R. Woo, A. Sardet, J. Venara, M. Ben Mosbah, R. Abou Khalil, Z. El Bitar, Demonstration of coded-aperture fast-neutron imaging based on Timepix detector, Nucl. Instrum. Methods A 954 (2020) 161373.

[134] C.M. Whitney, L. Soundara-Pandian, E.B. Johnson, S. Vogel, B. Vinci, M. Squillante, J. Glodo, J.F. Christian, Gamma—neutron imaging system utilizing pulse shape discrimination with CLYC, Nucl. Instrum. Methods A 784 (2015) 346—351.